Optics Letters

Continuous-wave optically pumped green perovskite vertical-cavity surface-emitter

Mohd Sharizal Alias,[1] Zhixiong Liu,[2] Abdullah Al-atawi,[1] Tien Khee Ng,[1] Tom Wu,[2] and Boon S. Ooi[1,*]

[1]King Abdullah University of Science & Technology (KAUST), Photonics Laboratory, Thuwal 23955-6900, Saudi Arabia
[2]King Abdullah University of Science & Technology (KAUST), Materials Science and Engineering, Thuwal 23955-6900, Saudi Arabia
*Corresponding author: boon.ooi@kaust.edu.sa

Received 28 July 2017; revised 17 August 2017; accepted 17 August 2017; posted 17 August 2017 (Doc. ID 303290); published 13 September 2017

We report an optically pumped green perovskite vertical-cavity surface-emitter operating in continuous-wave (CW) with a power density threshold of ~89 kW/cm^2. The device has an active region of $CH_3NH_3PbBr_3$ embedded in a dielectric microcavity; this feat was achieved with a combination of optimal spectral alignment of the optical cavity modes with the perovskite optical gain, an adequate *Q*-factor of the microcavity, adequate thermal stability, and improved material quality with a smooth, passivated, and annealed thin active layer. Our results signify a way towards efficient CW perovskite emitter operation and electrical injection using low-cost fabrication methods for addressing monolithic optoelectronic integration and lasing in the green gap. © 2017 Optical Society of America

OCIS codes: (140.3945) Microcavities; (160.4670) Optical materials.

https://doi.org/10.1364/OL.42.003618

Green lasers are attractive for applications in solid-state lighting and displays, underwater communications, astronomy tracking, and spectroscopy [1]. Most commercial green lasers use an indirect approach of second-harmonic generation from near-infrared (NIR) lasers [1–3]. Lasers using a direct approach such as a vertical-cavity surface-emitting laser (VCSEL) are more desirable. It can lase with a low operating threshold because the cavity volume is small (the active region typically has a thickness of about a wavelength and a volume that is three orders of magnitude smaller than an edge-emitting laser) and is embedded between highly reflective distributed Bragg reflectors (DBRs) to form the vertical cavity [4]. Moreover, since the laser beam emission is perpendicular to the surface, it can be fabricated economically (e.g., on-wafer test and high-density 2D arrays).

The emergence of hybrid perovskites for light-emitters [5–8], which combine the strengths of inorganic (e.g., high-crystallinity and high-carrier mobility, and efficient luminescence) and organic materials (e.g., economical processing, substrate flexibility, and wavelength tunability) is promising for resolving the lasing green gap. Attempts using other materials such as III-nitride compounds [2,3], suffer from material polarization and piezoelectric fields, and high-quality crystals are difficult to grow [2,3,9].

Green lasing in the amplified spontaneous emission (ASE) and stimulated emission (SE) regimes has been demonstrated using various $APbX_3$ hybrid perovskites, where A denotes CH_3NH_3, $CH(NH_2)_2$, or Cs cations and X is a Br anion. These approaches used hybrid perovskites in the form of powders with vertical cavities [10], cavity-free thin films [11,12], crystals with vertical cavities [13], microdisks/plates with whispering gallery modes (WGMs) [14,15], micro/nanowires with Fabry–Perot (FP) cavities [16,17] and gratings [18], micro/nanorods with FP cavities [19], cavity-free colloidal quantum dots [20] and WGMs [21], colloidal nanocrystals with WGMs [22], FP cavities [23], and vertical cavities [24]. Compared to ASE, SE typically has a narrower linewidth and obvious threshold, and exhibits beam divergence and polarization [25]. Concerning vertical-cavity approaches, only a few green devices using perovskite powders, crystals, and nanocrystals were reported for ASE [10,13] and SE [24] regimes. However, thick perovskite active layers were used without any optical waveguiding heterostructures and, thus, no cavity resonances were properly obtained. Moreover, the formation of the cavities by cast-capping (i.e., casting a perovskite solution on a DBR substrate and then capping it with another DBR and leaving it to dry for bonding) [10,13,24] is neither uniform nor scalable, which led to high operating thresholds and emission wavelength fluctuations [13].

All perovskites green-light emitters mentioned above [10,11,13–24] were optically pumped using ultrashort pulses (typically, femtoseconds). An optically pumped NIR perovskite laser using longer pulses (nanoseconds) was recently demonstrated [26], but it was operated in a cryogenic environment. A similar attempt was also reported for an NIR perovskite VCSEL [27]. Achieving lasing using continuous-wave (CW) optical pumping would be a major step towards realizing a perovskite-based CW electrically pumped laser.

Here, we demonstrate a CW optically pumped green perovskite vertical-cavity surface-emitter operating at room temperature (RT) by embedding a heterostructured active region of $CH_3NH_3PbBr_3$ thin films in a vertical cavity formed by

dielectric DBRs. The perovskite layer was synthesized and deposited, as previously reported [28]. Figure 1(a) shows the x-ray diffraction (XRD) spectra of $CH_3NH_3PbBr_3$ thin films on a single-crystal sapphire which are consistent with the literature of $CH_3NH_3PbBr_3$ [29,30] and sapphire [31]. The scanning electron microscopy (SEM) micrograph (inset) shows void-free and randomly oriented crystalline micrograins deposited on the DBR as the substrate. The atomic force microscopy (AFM) line-scan (inset) shows that the thickness of the $CH_3NH_3PbBr_3$ thin films is ~82 nm. The RT absorption and photoluminescence (PL) spectra in Fig. 1(b) exhibit an absorption edge near the optical bandgap of ~2.33 eV, as calculated using the Tauc plot (inset). The PL spectrum shows a peak at an emission wavelength of ~532 nm with a full-width at half-maximum (FWHM) of ~20 nm.

To form the vertical-cavity device, a heterostructured active region composed of $CH_3NH_3PbBr_3$/polymethyl methacrylate (PMMA) thin films with a total thickness of one wavelength was embedded between dielectric DBRs composed of SiO_2 and Si_3N_4 layers of a quarter-wavelength thickness as the low- and high-refractive index (RI) layers, respectively. The dielectric layers for the DBRs were deposited using plasma-enhanced chemical vapor deposition. The bottom DBR composing 14 pairs of SiO_2/Si_3N_4 layers was deposited on a single-crystal sapphire substrate at a temperature of 300°C. The top DBR (eight pairs of SiO_2/Si_3N_4 layers) was deposited at a low temperature [60°C] to preserve and anneal the $CH_3NH_3PbBr_3$ thin films simultaneously. Prior to device fabrication, the potential lasing wavelength was examined using a previously described pulsed-pumping setup with an ultrashort femtosecond laser [10]. Using a pristine sample of $CH_3NH_3PbBr_3$ thin films on single crystal sapphire, ASE was observed at a wavelength of ~541 nm with a FWHM of ~5.3 nm [see Fig. 2(a)] for a pumping fluence above the threshold (~30 μJ/cm^2). To ensure that the active region and DBRs had the desired

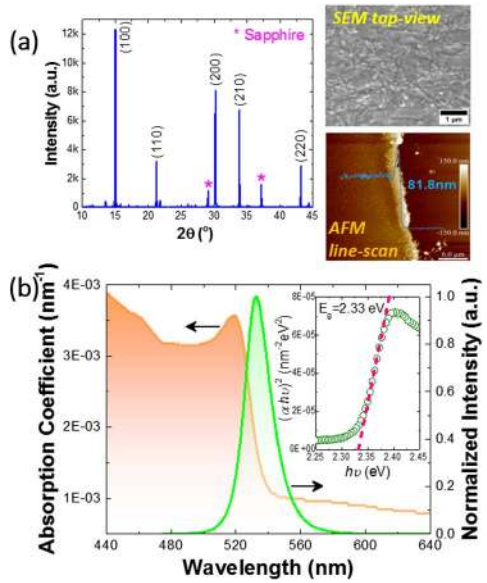

Fig. 1. Material analysis of $CH_3NH_3PbBr_3$ thin films showing (a) an XRD spectrum with SEM (top right) and AFM (bottom right) images, and (b) absorption coefficient and PL spectra with the Tauc plot (inset).

thicknesses at the targeted wavelength of 541 nm, RI measurements using spectroscopic ellipsometry were conducted, as shown in Fig. 2(b). The details of the experiment and fitting models can be found in earlier work [32]. Figure 2(c) displays the reflectivity spectra for the DBRs and shows that at 541 nm, the reflectivity for the top and bottom DBRs is ~85.7% and ~99.9%, respectively. The reflectivity of the top DBR is smaller because it has a lesser number of DBR pairs to ensure that light is emitted out of the surface. Furthermore, the SEM cross-sectional micrograph (inset) shows that the morphology of the top DBR is not uniform and has rougher interfaces compared to the bottom DBR, which is partly due to the lower deposition temperature. Nevertheless, the achieved reflectivity is considered to be high. The SEM cross-sectional micrograph of the entire perovskite vertical-cavity device is shown in Fig. 2(d). The heterostructured active region composed of $CH_3NH_3PbBr_3$/PMMA thin films is shown in the inset. Figure 2(e) shows the reflectivity and PL spectra (using CW optical pumping from a 325 nm He-Cd laser) measured on the full perovskite vertical-cavity device. The cavity resonance mode is obtained at $\lambda \sim 541$ nm with a FWHM of $\Delta\lambda \sim 2.67$ nm (at a pumping power density of ~6.8× threshold). The cavity mode dip in the reflectivity curve was found at the emission peak wavelength, indicating that resonant transmission was acquired for the device, i.e., the perovskite emission peak is well aligned with the microcavity formed. The cavity quality, i.e., Q-factor was estimated using $\lambda/\Delta\lambda$ formulation from the PL emission which is ~203.

Figure 3(a) shows the integrated PL intensity as a function of power density (log-log scale, with inset showing the linear scale) for the green perovskite vertical-cavity emitter at RT. The device was optically pumped using a 325 nm He-Cd laser under CW operation with a beam power of ~8 mW. A 15× near UV objective lens with a numerical aperture of 0.32 was used to excite an area of approximately 1.2 μm and to collect light emission from the samples in the normal direction. For reliability, all PL spectra were collected at three different positions and averaged. Figure 3(b) exhibits the PL spectra for several CW pumping power densities below and above the power density threshold of $P_{th} \sim 89$ kW/cm^2. The threshold is slightly observed, similar to those reported for other perovskite ASE devices [22,33]. The FWHM of the spectrum collapsed from ~24 nm below the threshold to ~2.67 nm above the threshold, as shown in Fig. 3(a). The emission is considered to be enhanced ASE. Typically, most $CH_3NH_3PbBr_3$-based lasing devices have been reported to have FWHMs of <1 nm [16–18], and FWHMs for ASE devices have been ~5 nm [11,12,20]. No significant degree of polarization was shown when the present device was tested with polarization measurement to suggest lasing. Nevertheless, a first enhanced ASE for a perovskite device is obtained here under CW pumping. Several attempts for perovskite lasing [24,26,27] and ASE [12,33,34] under longer pulse (nanosecond) pumping were reported recently to understand the challenges that hinder CW optical pumping. Among the challenges to be overcome are Auger recombination, material quality, and thermal stability [6–8,27,34]. High Auger recombination coefficients and material defects contribute to higher ASE and the lasing threshold in the form of non-radiative loss [27,34], whereas thermal stability is required to sustain heating introduced from longer optical pump pulses since perovskites exhibit poor

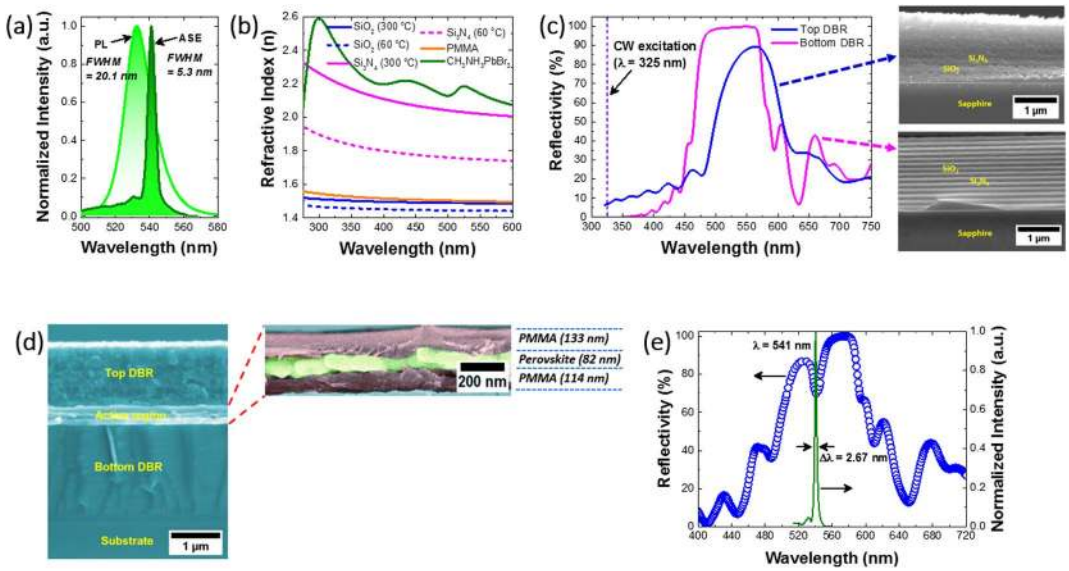

Fig. 2. Measurements showing (a) ASE and PL spectra of a pristine sample, i.e., $CH_3NH_3PbBr_3$ thin films deposited on a single-crystal sapphire substrate, (b) wavelength-dependent RI spectra for each material used for the fabrication of the perovskite vertical-cavity device, (c) reflectivity spectra for the top and bottom DBRs with the corresponding SEM cross sections (inset), (d) SEM cross section of the full device structure with the heterostructured active region (inset), and (e) reflectivity and PL spectra for the full device with the cavity resonance wavelength indicated.

thermal conductivity of ~0.25–0.5 W/mK [35]. All of these challenges can be addressed by appropriate material and device engineering.

To counter Auger recombination, the perovskite layer can be embedded within a cavity structure with a small mode volume and sufficient Q-factor. The enhancement of spontaneous emission by the Purcell effect can overcome Auger recombination [36]. Figure 4(a) shows the standing wave profile for our device simulated using a transfer-matrix method solver based on the measured RI and thickness of each layer. By optimally designing the spectral alignment of the cavity optical modes and the gain, i.e., the perovskite layer at the antinode of the standing wave, the coupling of photons was enhanced, and the ASE threshold was obtained. The heterostructured active region ($CH_3NH_3PbBr_3$/PMMA) in our device helps to realize this and acts as a waveguiding layer. We have fabricated two control devices: one without the PMMA spacers and a thicker perovskite layer (control 1) and one with half a cavity (control 2). Neither device showed any ASE threshold under

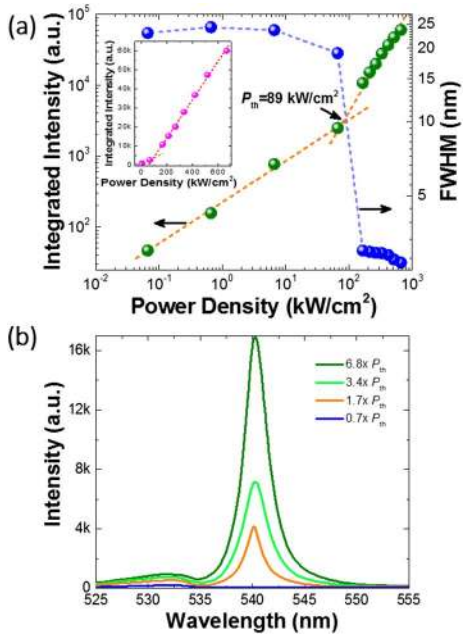

Fig. 3. Device characteristics showing (a) integrated PL intensity and FWHM as a function of power density (log–log scale with inset shown in linear scale), and (b) evolution of emission spectra at different optical pumping power densities below and above the threshold.

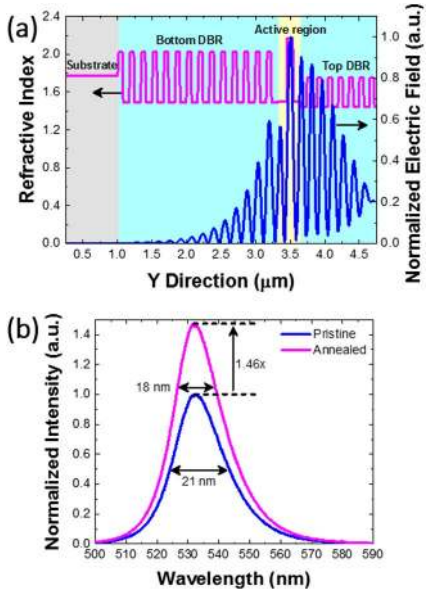

Fig. 4. (a) RI and optical standing wave profile across the device. (b) Improvement in PL characteristics with annealing.

the same CW pumping. To improve the material quality, the top DBR was purposely deposited at a low temperature of 60°C in order to concurrently preserve and anneal the $CH_3NH_3PbBr_3$ layer underneath. This resulted in a PL enhancement factor of 1.46 and a narrowing of the FWHM by ~3 nm, as shown in Fig. 4(b). We have previously reported increased device efficiency for $CH_3NH_3PbBr_3$ solar cells and photodetectors when annealing was performed at this temperature [37]. The use of PMMA in the heterostructured active region also reduced the ASE threshold by half [12] due to the smoother surface, surface passivation, and waveguiding effects. Furthermore, by heterostructure engineering, only a nanoscale perovskite layer is required (~82 nm) for our device compared to the larger thickness of microscales required for other devices [10,13,24]. A thin perovskite layer is essential to form heterostructures and to reduce material defects and thermal resistance [34]. For thermal management, we used a single-crystal sapphire substrate that has a thermal conductivity of ~46 W/mK [38]. Usage of this substrate together with the dielectric DBRs (with thermal conductivity of ~1.14 W/mK [39]) helped to minimize the thermal resistivity of the perovskite layer. Recently, it was speculated that the excitation power density required for $CH_3NH_3PbI_3$ hybrid perovskites to lase under CW pumping would be $P_{th} \sim 14$ kW/cm^2 [27]. In addition to improving the material quality, thermal stability, and Q-factor of the microcavity, further device engineering such as forming an optical guiding by mesa patterning [40,41] or lateral confinement [42,43] can lower the device threshold so that CW lasing is feasible.

In summary, we have demonstrated a CW optically pumped green perovskite vertical-cavity surface-emitter operating at RT. This feat was enabled by a heterostructured active region, optimal spectral alignment of the cavity optical modes and the perovskite gains, a sufficient Q-factor of the microcavity, good material quality obtained with a passivated and annealed thin layer, and adequate thermal stability of the device. Our findings can pave the way towards CW electrical injection perovskite lasers using monolithic fabrication methods and addressing the lasing green gap.

Funding. King Abdullah University of Science and Technology (KAUST) (BAS/1/1614-01-01); King Abdulaziz City for Science and Technology (KACST) (TIC R2-FP-008).

REFERENCES

1. W. P. Risk, T. R. Gosnell, and A. V. Nurmikko, *Compact Blue-Green Laser* (Cambridge University, 2003).
2. D. Sizov, R. Bhat, and C. E. Zah, J. Lightwave Technol. **30**, 679 (2012).
3. A. Masahiro, Jpn. J. Appl. Phys. **53**, 100207 (2014).
4. K. Iga, IEEE J. Sel. Top. Quantum Electron. **6**, 1201 (2000).
5. S. D. Stranks and H. J. Snaith, Nat. Nanotechnol. **10**, 391 (2015).
6. B. R. Sutherland and E. H. Sargent, Nat. Photonics **10**, 295 (2016).
7. S. A. Veldhuis, P. P. Boix, N. Yantara, M. Li, T. C. Sum, N. Mathews, and S. G. Mhaisalkar, Adv. Mater. **28**, 6804 (2016).
8. G. Li, M. Price, and F. Deschler, APL Mater. **4**, 091507 (2016).
9. S. P. DenBaars, D. Feezell, K. Kelchner, S. Pimputkar, C.-C. Pan, C.-C. Yen, S. Tanaka, Y. Zhao, N. Pfaff, R. Farrell, M. Iza, S. Keller, U. Mishra, J. S. Speck, and S. Nakamura, Acta Mater. **61**, 945 (2013).
10. D. Priante, I. Dursun, M. S. Alias, D. Shi, V. A. Melnikov, T. K. Ng, O. F. Mohammed, O. M. Bakr, and B. S. Ooi, Appl. Phys. Lett. **106**, 081902 (2015).
11. N. Arora, M. I. Dar, M. Hezam, W. Tress, G. Jacopin, T. Moehl, P. Gao, A. S. Aldwayyan, B. Deveaud, M. Grätzel, and M. K. Nazeeruddin, Adv. Funct. Mater. **26**, 2846 (2016).
12. J. Li, J. Si, L. Gan, Y. Liu, Z. Ye, and H. He, ACS Appl. Mater. Interfaces **8**, 32978 (2016).
13. V.-C. Nguyen, H. Katsuki, F. Sasaki, and H. Yanagi, Appl. Phys. Lett. **108**, 261105 (2016).
14. Q. Liao, K. Hu, H. Zhang, X. Wang, J. Yao, and H. Fu, Adv. Mater. **27**, 3405 (2015).
15. J. Feng, X. Yan, Y. Zhang, X. Wang, Y. Wu, B. Su, H. Fu, and L. Jiang, Adv. Mater. **28**, 3732 (2016).
16. Z. Gu, K. Wang, W. Sun, J. Li, S. Liu, Q. Song, and S. Xiao, Adv. Opt. Mater. **4**, 472 (2015).
17. H. Zhu, Y. Fu, F. Meng, X. Wu, Z. Gong, Q. Ding, M. V. Gustafsson, M. T. Trinh, S. Jin, and X. Y. Zhu, Nat. Mater. **14**, 636 (2015).
18. K. Y. Wang, Z. Y. Gu, S. Liu, W. Z. Sun, N. Zhang, S. M. Xiao, and Q. H. Song, J. Phys. Chem. Lett. **7**, 2549 (2016).
19. H. Zhou, S. Yuan, X. Wang, T. Xu, X. Wang, H. Li, W. Zheng, P. Fan, Y. Li, L. Sun, and A. Pan, ACS Nano **11**, 1189 (2017).
20. J. Pan, S. P. Sarmah, B. Murali, I. Dursun, W. Peng, M. R. Parida, J. Liu, L. Sinatra, N. Alyami, C. Zhao, E. Alarousu, T. K. Ng, B. S. Ooi, O. M. Bakr, and O. F. Mohammed, J. Phys. Chem. Lett. **6**, 5027 (2015).
21. Y. Wang, X. M. Li, J. Z. Song, L. Xiao, H. B. Zeng, and H. D. Sun, Adv. Mater. **27**, 7101 (2015).
22. S. Yakunin, L. Protesescu, F. Krieg, M. I. Bodnarchuk, G. Nedelcu, M. Humer, G. De Luca, M. Fiebig, W. Heiss, and M. V. Kovalenko, Nat. Commun. **6**, 8056 (2015).
23. E. Lafalce, C. Zhang, Y. Zhai, D. Sun, and Z. V. Vardeny, J. Appl. Phys. **120**, 143101 (2016).
24. Y. Wang, X. Li, V. Nalla, H. Zeng, and H. Sun, Adv. Funct. Mater. **27**, 1605088 (2017).
25. I. D. W. Samuel, E. B. Namdas, and G. A. Turnbull, Nat. Photonics **3**, 546 (2009).
26. Y. Jia, R. A. Kerner, A. J. Grede, A. N. Brigeman, B. P. Rand, and N. C. Giebink, Nano Lett. **16**, 4624 (2016).
27. S. Chen, C. Zhang, J. Lee, J. Han, and A. Nurmikko, Adv. Mater. **29**, 1604781 (2017).
28. C. Ma, Y. Shi, W. Hu, M.-H. Chiu, Z. Liu, A. Bera, F. Li, H. Wang, L.-J. Li, and T. Wu, Adv. Mater. **28**, 3683 (2016).
29. A. Kojima, K. Teshima, Y. Shirai, and T. Miyasaka, J. Am. Chem. Soc. **131**, 6050 (2009).
30. J. H. Noh, S. H. Im, J. H. Heo, T. N. Mandal, and S. I. Seok, Nano Lett. **13**, 1764 (2013).
31. J. Engel and H. L. Tuller, Phys. Chem. Chem. Phys. **16**, 11374 (2014).
32. M. S. Alias, I. Dursun, M. I. Saidaminov, E. M. Diallo, P. Mishra, T. K. Ng, O. M. Bakr, and B. S. Ooi, Opt. Express **24**, 16586 (2016).
33. S. D. Stranks, S. M. Wood, K. Wojciechowski, F. Deschler, M. Saliba, H. Khandelwal, J. B. Patel, S. J. Elston, L. M. Herz, M. B. Johnston, A. P. H. J. Schenning, M. G. Debije, M. K. Riede, S. M. Morris, and H. J. Snaith, Nano Lett. **15**, 4935 (2015).
34. M. Cadelano, V. Sarritzu, N. Sestu, D. Marongiu, F. Chen, R. Piras, R. Corpino, C. M. Carbonaro, F. Quochi, M. Saba, A. Mura, and G. Bongiovanni, Adv. Opt. Mater. **3**, 1557 (2015).
35. A. Pisoni, J. Jaćimović, O. S. Barišić, M. Spina, R. Gaál, L. Forró, and E. Horváth, J. Phys. Chem. Lett. **5**, 2488 (2014).
36. S. Gupta and E. Waks, Opt. Express **22**, 3013 (2014).
37. B. Murali, E. Yengel, W. Peng, Z. Chen, M. S. Alias, E. Alarousu, B. S. Ooi, V. Burlakov, A. Goriely, M. Eddaoudi, O. M. Bakr, and O. F. Mohammed, J. Phys. Chem. Lett. **8**, 137 (2017).
38. E. R. Dobrovinskaya, L. A. Lytvynov, and V. Pishchik, *Sapphire: Material, Manufacturing, Applications* (Springer, 2009).
39. S. W. Fong, A. Sood, L. Chen, N. Kumari, M. Asheghi, K. E. Goodson, G. A. Gibson, and H.-S. P. Wong, J. Appl. Phys. **120**, 015103 (2016).
40. M. S. Alias, I. Dursun, D. Shi, M. I. Saidaminov, E. M. Diallo, D. Priante, T. K. Ng, O. M. Bakr, and B. S. Ooi, J. Vac. Sci. Technol. B **33**, 051207 (2015).
41. M. S. Alias, Y. Yang, T. K. Ng, I. Dursun, D. Shi, M. I. Saidaminov, D. Priante, O. M. Bakr, and B. S. Ooi, J. Phys. Chem. Lett. **7**, 137 (2016).
42. S. M. Mitani, P. K. Choudhury, and M. S. Alias, Optik **119**, 373 (2008).
43. M. S. Alias, S. Shaari, and S. M. Mitani, Laser Phys. **20**, 806 (2010).

115.164.60.185 {ts '2017-09-12 19:53:04'}